3D Modeling of Thin-Walled Structures

Session Organizers: Manfred BISCHOFF, Ekkehard RAMM (University of Stuttgart)

Plenary Lecture: Abstract, Slides and Video
Modeling of shells with three-dimensional finite elements
Manfred BISCHOFF (University of Stuttgart)

Keynote Lecture
Modeling and mesh error estimates for plates and thick shells
Uros BOHINC, Boštjan BRANK (University of Ljubljana), Adnan IBRAHIMBEGOVIC, (ENS-Cachan)*

Physical applications for a nonlinear micropolar formulation on shells
Ingo MÜNCH, Werner WAGNER (Universität Karlsruhe), Patrizio NEFF (TU Darmstadt)*

Utilization of the assumed natural strain method in a surface-related solid-shell element
Bernd W. ZASTRAU, Rainer SCHLEBUSCH (TU Dresden)*

Dimensional adaptivity in finite element simulation of sheet metal forming
Dmitry LEDENTSOV, Alexander DÜSTER, Ernst RANK (TU München), Ingo HEINLE, Wolfram VOLK, Marcus WAGNER (BMW Group, München)*

For multiple-author papers:
Contact author designated by *
Presenting author designated by underscore

Proceedings of the 6th International Conference on
Computation of Shell and Spatial Structures
IASS-IACM 2008: "Spanning Nano to Mega"
28-31 May 2008, Cornell University, Ithaca, NY, USA
John F. ABEL and J. Robert COOKE (eds.)

Modeling of shells with three-dimensional finite elements

Manfred BISCHOFF

Institut für Baustatik und Baudynamik, Universität Stuttgart
Pfaffenwaldring 7, D-70550 Stuttgart, Germany
bischoff@ibb.uni-stuttgart.de

Abstract

Some aspects of three-dimensional analysis of shells are discussed, comparing 3d-shell formulations, surface oriented shell formulations and three-dimensional solid elements ("bricks"). Comparison is made with respect to theoretical formulation, finite element technology and consistency. Advantages and drawbacks of the different concepts are discussed, distinguishing the case of thin shells, where locking effects play a prominent role, and the analysis of three-dimensional structures ("very thick" shells). In this context a fundamental dilemma appears, namely the impossibility to design an element which is completely free of locking and passes the patch test at the same time.

1. Introduction

Finite element analysis of shells is a standard procedure in many engineering applications. Throughout the past fifteen years significant progress has been made in the field of three-dimensional shell theories and related finite elements (also called "solid shell" elements). The main benefits are approximate consideration of three-dimensional stress states, ease of implementation of three-dimensional constitutive laws and simplicity (no rotational degrees of freedom involved).

Sometimes application of shell finite elements is totally abandoned in favor of a discretization with three-dimensional solid finite elements. Standard 3d-solid finite elements, however, are often not suited to predict the behavior of shells properly. Locking effects may lead to significant errors for thin shells. Even well-established "locking-free" solid elements may fail in thin shell analysis. The problem can be avoided by transferring concepts of finite element technology from (3d) shell elements to solid elements.

A particularly interesting phenomenon in this context is *trapezoidal locking* (also called *curvature thickness locking* in the context of 3d-shell elements) and its relationship to passing the constant stress patch test. There are strong indications that obtaining a locking-free formulation and passing the patch test are mutually exclusive (a result already anticipated by Richard MacNeal in a discussion about distortion sensitivity of finite elements).

2. Three different archetypes of three-dimensional elements for shell analysis

Without going into technical details of mathematical formulations, three different philosophies for designing finite elements which are feasible for both thick and thin shell analysis, using unmodified three-dimensional constitutive laws are described in this section (see Figure 1 for an illustration).

3d-shell finite elements have become popular (particularly in Germany) at the beginning of the 90s, the works of Simo et al. [4] and Büchter et al. [4] being two of the decisive pioneering contributions. They rely on the classical concept of a mid-surface, equipped with displacement degrees of freedom, rotations (or difference displacements) as well as some higher order parameters, for instance describing the thickness change of the shell. A typical representative of this class is a so-called *7-parameter formulation*, utilizing three displacements of the mid-surface, three components of a difference vector (naturally including a constant thickness stretch) plus one additional strain (or displacement) parameter to realize a linear distribution of transverse normal strains. The latter is necessary to avoid *Poisson thickness locking* or, in other terms, to make the formulation asymptotically correct for bending.

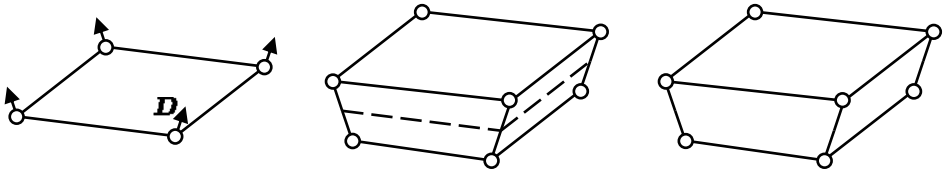

Figure 1: 3d-shell, surface oriented shell and "shell-like" 3d-solid

Unless the three-dimensional constitutive equations are somehow manipulated, all strain components need to be linear through the thickness in order to correctly model bending. In this spirit, quadratic terms are not needed for an asymptotically correct shell model and they are usually dropped from the formulation. Contribution of these higher order terms to the strain energy is negligible in most cases. This assumption is commonplace for practically all classical and three-dimensional shell models.

The mechanical ingredients of *surface oriented* shell formulations are identical to those of 3d-shells. The decisive difference is the usage of a three-dimensional parameterization of geometry and displacements with *absolute* values for position vectors and displacements rather than working with a director field $\boldsymbol{D}$ and difference displacements $\boldsymbol{w}$, see Figure 2. Surface oriented shell finite elements may be seen as hybrids of three-dimensional finite elements and shell elements. From the former they inherit their "outer appearance", i.e. geometry and nodal degrees of freedom. And from the latter the "inner life" is deduced, particularly the use of stress *resultants* (membrane forces, bending moments etc.), rather than stresses and the aforementioned reduction strains to linear functions in thickness direction.

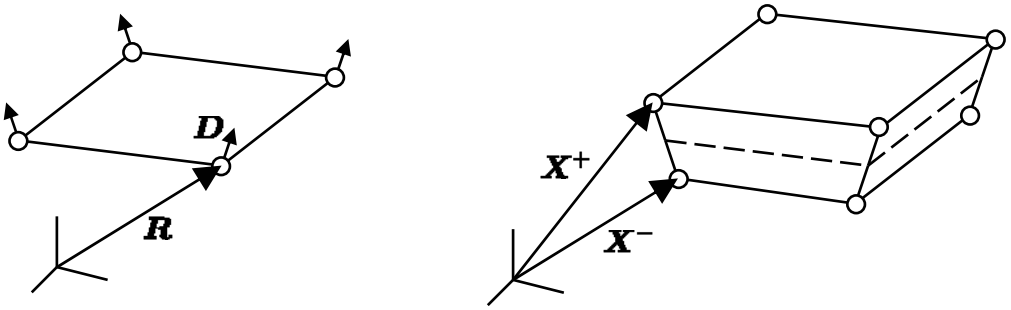

Figure 2: "classical" 3d-shell versus surface oriented 3d-shell

The concept of a surface-oriented shell model described in the previous section implies the question why not simply using 3d-elements for shell analysis. The nodal degrees of freedom are exactly the same and the 7th parameter is naturally included in many 3d-solid finite elements by certain means of element technology which are needed to avoid volumetric locking (EAS, Simo and Rifai [4]). The decisive differences of three-dimensional solid elements compared to three-dimensional (or surface oriented) shell elements are

1. that there are no distinct "in-plane" and "thickness" directions and
2. three-dimensional strains and stresses, rather than "resultants" are used, i.e. there are no separate expressions for membrane strains, curvatures, bending moments or transverse shear forces.

As a consequence, in a three-dimensional finite element the quadratic terms of the through-the-thickness strain distribution are not skipped – they *cannot* be skipped, because they do not appear separately. This is not a disadvantage because it does not affect computational cost. It may be even advantageous to have these terms included, as we will see later.

There is, however, a drawback in comparison to shell elements: From the point of view of element technology it is desirable to distinguish in-plane and out-of-plane strain and stress components, (e.g. when special formulations ought to be applied to avoid *transverse* shear locking or trapezoidal locking) as well as constant and linear ones (e.g. membrane and bending strains when membrane locking ought to be avoided). In fact, the crucial problem is trapezoidal locking (related to transverse normal strains) as will be demonstrated in the next section.

3. Trapezoidal locking and the patch test

We compare, in a numerical experiment, performance of state of the art solid elements and shell elements. A cylindrical shell with clamped boundaries is subject to uniform external pressure. A linear pre-buckling analysis is performed, based on solving the corresponding eigen value problem. Two different setups are considered: a relatively thick shell, with a radius-to-thickness ratio of 100 and a thin shell with slenderness 500. The commercial finite element package ANSYS is used as solver. The solid elements implemented in ANSYS use the enhanced assumed strain method, representing widely used, and state of the art brick elements. Comparison is made to a solution using conventional Kirchhoff-Love type shell elements which are free from locking for the problem at hand (similar results are obtained with well-formulated 3d-shell elements).

	mesh	shell elements	solid elements
thick shell	coarse	$\lambda_{crit.} = 1.02$	$\lambda_{crit.} = 1.7$
	fine	$\lambda_{crit.} = 1.0$ (reference)	$\lambda_{crit.} = 1.02$
thin shell	coarse	$\lambda_{crit.} = 1.02$	$\lambda_{crit.} = 13.0$
	fine	$\lambda_{crit.} = 1.0$ (reference)	$\lambda_{crit.} = 1.7$

Table 1: Critical load factors for thick and thin shell, fine and coarse meshes

The numerical results, normalized with respect to the fine mesh shell solution are summarized in Table 1. The coarse meshes use 4608 degrees of freedom (in both shell and solid discretizations) and the fine mesh involves 18816 d.o.f. It can be seen that the coarse mesh solution using shell elements is already satisfactory, while the coarse mesh solution with solid elements is unacceptable in both cases (thick and thin cylinder). Moreover, the absolute errors are much larger for the thin cylinder in the solid element solutions – a typical symptom of locking. Note, that even for the fine mesh the critical load is overestimated by 70 %. Figure 3 shows that the solid elements do not only overestimate the buckling load but also predict a wrong buckling pattern.

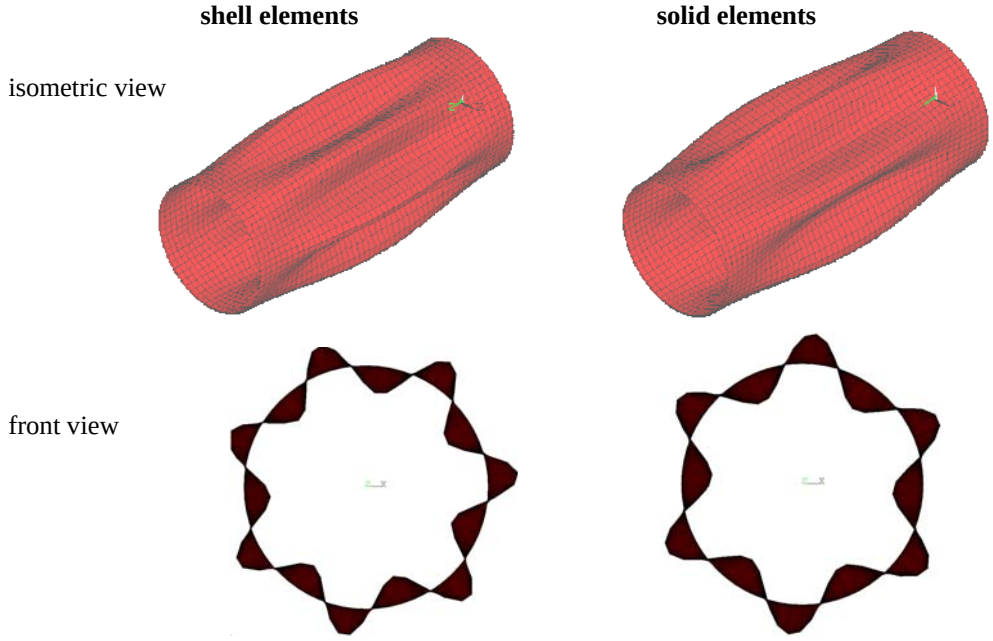

Figure 3: Comparison of buckling modes for shell elements and solid elements

Analyzing the problem setup and the involved element formulations one can identify trapezoidal locking as the reason for the observed behavior. Within a three-dimensional or surface oriented shell formulation it can be avoided following the idea of Betsch et al. [4] (see also Bischoff and Ramm [4]), modifying the constant part of

the transverse normal strains ε_{33} by an ANS formulation. As there is no "transverse" direction in a 3d-solid, transferring this concept is not straightforward. If one strives to keep element technology "isotropic", all normal strain components ought to be modified accordingly. This works fine for the numerical experiment documented in this section, but the resulting elements fail to pass the constant strain patch test. Strictly speaking, this means that these elements are not consistent and thus not convergent – a fact that is mostly considered unacceptable. The same holds for typical methods to avoid transverse shear locking.

We conclude that there is no way around an "anisotropic" element technology for 3d-solids, if these are expected to work as well as (3d) shell elements in the case of thin shells. This means that a certain thickness direction has to be nominated and the finite element formulation is adapted accordingly. If transverse shear strains and transverse normal strains are treated such that transverse shear locking and trapezoidal locking are avoided, 3d-solid elements may be used as efficiently as 3d-shell elements for thin shell analysis. These elements pass the patch test as long as the elements are distorted "in-plane", but still not in general three-dimensional situations. To be more precise: Constant strain states cannot be exactly represented if the thickness direction is not orthogonal to the other two directions.

The special treatment of transverse normal strains to avoid trapezoidal locking is one of the reasons for this problem. This observation is closely related to a discussion about distortion sensitivity of finite elements and passing the patch test, put forward by Richard MacNeal [4]. Removing these "tricks" from the element formulation leads to an element that passes the patch test (of course, trapezoidal locking re-enters the formulation).

For a surface oriented shell element the patch test is still not passed in this case. The reason is omitting the quadratic terms of the strain distribution trough the thickness. These are needed for exact representation of constant stress states for arbitrary meshes, because the metric is changing through the thickness.

One way out of this dilemma may be to accept the fact that the elements do not pass the patch test and favor formulations which are locking-free. Consistency, and thus convergence, may be achieved in a weaker sense by ensuring that those element distortions which are responsible for not passing the patch test vanish with mesh refinement. As these are related to deviation of the shell director from the shell normal, this seems to be a feasible approach.

3. Summary

Formulation of locking free 3d-solid elements for shells still has potential for improvement. Avoiding all locking effects and passing the patch test at the same time seem to be mutually exclusive. Standard "locking-free" 3d-solid elements usually suffer from trapezoidal locking and are therefore not suited for general shell analysis. The situation can be improved with an anisotropic element technology. Surface oriented shell elements use stress resultants and thus methods of element technology may be applied more purposeful.

References

[1] P. Betsch. F. Gruttmann, E. Stein. A 4-node finite shell element for the implementation of general hyperelastic 3d-elasticity at finite strains. *Computer Methods in Applied Mechanics and Engineering*, **130**:75-79, 1995.

[2] M. Bischoff, E. Ramm. Shear deformable shell elements for large strains and rotations. *International Journal for Numerical Methods in Engineering*, **40**:4427-4449, 1997.

[3] N. Büchter, E. Ramm, D. Roehl. Three-dimensional extension of non-linear shell formulation based on the enhanced assumed strain concept. *International Journal for Numerical Methods in Engineering* **37**:2551-2568, 1994.

[4] R. MacNeal. *Finite Elements: Their Design and Performance*. Marcel Dekker, 1994.

[5] J.C. Simo, S. Rifai. A class of mixed assumed strain methods and the method of incompatible modes. *International Journal for Numerical Methods in Engineering*, **29**:1595-1638, 1990.

[6] J.C. Simo, S. Rifai, D. Fox. On a stress resultant geometrically exact shell model. Part IV: variable thickness shells with through-the-thickness stretching. *Computer Methods in Applied Mechanics and Engineering*, **81**:91-126, 1989.

Proceedings of the 6th International Conference on
Computation of Shell and Spatial Structures
IASS-IACM 2008: "Spanning Nano to Mega"
28-31 May 2008, Cornell University, Ithaca, NY, USA
John F. ABEL and J. Robert COOKE (eds.)

Modelling and mesh error estimates for plates and thick shells

Uros BOHINC*, Boštjan BRANK* and Adnan IBRAHIMBEGOVIC**

* University of Ljubljana, FGG
Jamova 2, 1000 Ljubljana, Slovenia
bbrank@ikpir.fgg.uni-lj.si

**Ecole Normale Supérieure de Cachan
LMT, 61 av. du president Wilson, 94235 Cachan, France
adnan.ibrahimbegovic@lmt.ens-cachan.fr

Abstract

We present a methodology of a posteriori error estimation and adaptivity for modelling error for the problem of linear elastic plate bending. The basic idea is that for each finite element of the mesh, which is considered satisfying from the standpoint of the discretization error, a sufficiently refined plate bending model is chosen so that the modelling error is distributed nearly uniformly in all regular and disturbed areas of the plate.

We estimate the error in linear elastic plate bending by using implicit residual a posteriori modeling error estimator that is based on the representation of the weak form of the residual that includes equilibrated boundary tractions. When the boundary tractions are approximated by using solution of the coarse model, solution of the finer model is obtained by solving local element based Neumann problems. The model error estimator is defined in an energy norm from the difference of the internal forces of finer and coarse models.

The plate bending models that are considered are: discrete Kirchhoff model, Reissner-Mindlin model, higher order model that takes into account through-the-thickness stretching, and 3d solid model [1,2,3,4].

References

[1] Brank B., J.Korelc, A.Ibrahimbegovic, 'Nonlinear shell problem formulation accounting for though-the-thickness stretching and its finite element implementation', Computers and Structures, 80, 696-717, (2002)

[2] E. Stein, M. Rueter and S. Ohnimus, "Adaptive finite element analysis of solids and structures. Findings, problems and trends",Int. J. Numer. Meth. Engng., Vol. 60, pp. 103–138, (2004)

[3] J.T. Oden, S. Prudhomme, D.C. Hammerand and M.S. Kuczma, "Modeling error and adaptivity in nonlinear continumm mechanics",Comput. Methods Appl. Mech. Engrg., Vol. 190, pp. 6663–6684, (2001)

[4] U. Bohinc, A. Ibrahimbegovic and B. Brank, "Model adaptivity for finite element analysis of thin or thick plates based on equilibrated boundary stress resultants", Engineering Computations, in press, (2008)

Proceedings of the 6th International Conference on
Computation of Shell and Spatial Structures
IASS-IACM 2008: "Spanning Nano to Mega"
28-31 May 2008, Cornell University, Ithaca, NY, USA
John F. ABEL and J. Robert COOKE (eds.)

Physical applications for a nonlinear micropolar formulation on shells

Ingo MÜNCH*, Werner WAGNER, Patrizio NEFF

*Institut für Baustatik, Universität Karlsruhe (TH)
Kaiserstr. 12, 76131 Karlsruhe, Germany
ingo.muench@bs.uka.de

Abstract

As continuum theory with rotational degrees of freedom, the Cosserat theory is prominently used in shell formulations. But it is also used to regularize stress-concentrations in elasticity or shear-bands in elasto-plasticity. Further, a wide spectrum of material models, e.g. for soils, foams or composites are based on the Cosserat model. Even dislocated crystals are subjected to this theory. The reason for this wide range of applications is that the Cosserat continuum treats angular momentum as an explicit complementary principle. This is why couple-stresses and non-symmetric Cauchy-stresses are possible and fundamental for Cosserat models.

Although having this wide range of applications, it is fair to say that the Cosserat theory is not commonly accepted in comparison to the Boltzmann continuum. One reason may be, that Cosserat theory often leads to higher expenditures without a worth mentioning advantage. Moreover, by extending the kinematical equations through rotational degrees of freedom, the need for extended constitutive description appears. In this context discrepancies to the classical continuum act as a deterrent to the use of a Cosserat model. This paper highlights therefore the question of constitutive parameters.

In our formulation material parameters receive a maximum of options. One option include that Cosserat rotations $\bar{\mathbf{R}}$ are really independent of the deformation gradient $\mathbf{F}$. Beside the first Cosserat strain measure $\bar{\mathbf{U}} = \bar{\mathbf{R}}^T \mathbf{F}$, which appears in the internal energy density W_{mp}, we include a second strain measure, which is based on gradients of the rotation field $\bar{\mathbf{R}}$. This strain measure represents in fact the curvature of the substructure and gives rise to a nonlinear internal curvature energy density W_{curv}. It is of second order small when compared to the local strain energy W_{mp}. We present an application, where the model benefits from the Cosserat theory.

1. Introduction

Similar to the rotational degrees of freedom used in the algorithmic treatments of shells, the Cosserat continuum introduces an additional rotation field represented by $\bar{\mathbf{R}} \in \mathrm{SO}(3)$. This additional rotation field is coupled to the deformation $\boldsymbol{\Phi}$ through the strain measure

$$\bar{\mathbf{U}} := \bar{\mathbf{R}}^T \operatorname{Grad}[\boldsymbol{\Phi}] = \bar{\mathbf{R}}^T \mathbf{F} \quad , \quad \bar{\mathbf{U}} \in \mathrm{GL}^+(3) \quad \Leftrightarrow \quad \mathbf{F} = \bar{\mathbf{R}}\,\bar{\mathbf{U}} \quad . \tag{1}$$

We also define a specific curvature measure, which is only based on the rotation field

$$\mathfrak{C} = \operatorname{Curl}[\bar{\mathbf{R}}] \cdot \bar{\mathbf{R}} \quad . \tag{2}$$

For physical relevance of $\mathfrak{C}$ and its relation to dislocations see NEFF & MÜNCH [1].

The strain $\bar{\mathbf{U}}$ is possibly nonsymmetric and we emphasize this difference to classical symmetric strain measures. An additional kinematic $\hat{\mathbf{R}}$ can be identified as a consequence of really independent Cosserat rotations with

$$\hat{\mathbf{R}} = \bar{\mathbf{R}}^T \operatorname{polar}[\mathbf{F}] \quad , \quad \{\hat{\mathbf{R}} = \mathbb{1} \;\Rightarrow\; \bar{\mathbf{U}} \in \mathrm{Sym} \,|\, \bar{\mathbf{R}} = \operatorname{polar}[\mathbf{F}]\} \quad , \tag{3}$$

where $\operatorname{polar}[\mathbf{F}]$ is the orthogonal part of the polar decomposition of $\mathbf{F}$. This equation states, that the additional kinematic disappears if the Cosserat rotation $\bar{\mathbf{R}}$ coincides with the macroscopic rotation $\operatorname{polar}[\mathbf{F}]$. Then the strain $\bar{\mathbf{U}}$ is also symmetric and realizes the classical Biot's strain tensor.

The Cosserat continuum treats angular momentum as an explicit complementary principle. This is why couple-stresses and non-symmetric Cauchy-stresses are possible. The form of their appearance and interpretation depends on constitutive parameters. We introduce the inner strain energy density

$$W_{\mathrm{mp}}(\bar{\mathbf{U}}) = \mu\|\mathrm{sym}[\bar{\mathbf{U}} - \mathbb{1}]\|^2 + \mu_c\|\mathrm{skew}[\bar{\mathbf{U}}]\|^2 + \frac{\lambda}{4}\left((\det[\bar{\mathbf{U}}]-1)^2 + \left(\frac{1}{\det[\bar{\mathbf{U}}]}-1\right)^2\right) \quad , \tag{4}$$

which is consistent with classical elasticity theories having the Lamé parameters μ and λ.

Because of $\det[\bar{\mathbf{U}}] = \det[\bar{\mathbf{R}}^T\,\mathbf{F}] = \det[\mathbf{F}]$, rotations are in reality absent in the volumetric inner strain energy, as it is physically reasonable. Skewsymmetric parts of strain are penalized by the Cosserat couple modulus μ_c. Further, we introduce the inner curvature energy density

$$W_{\mathrm{curv}} := \frac{\mu}{q}\,(1 + 2\,L_c^2\,\|\mathfrak{C}\|^2)^{\frac{q}{2}}\,, \quad q > 3 \quad . \tag{5}$$

The internal length scale L_c acts as a torsional spring and penalizes a special form of gradient in the rotation field $\bar{\mathbf{R}}$. The couple modulus μ_c is not to be treated like a material parameter but like a modelling parameter. To explain this we discuss two borderline cases. For $\mu_c = \mu$ and $L_c = 0$ the Cosserat theory realizes the classical Biot model, see NEFF et al. [2]. This can be useful, if one strives for a classical elasticity formulation and couples algorithmically rotational degrees of freedom to the macroscopic deformation in a strong way. Thus, the inner kinematic $\hat{\mathbf{R}}$ vanishes and one excludes non-classical deformation modes. Nevertheless, the Cosserat rotation $\bar{\mathbf{R}}$ is algorithmically available for extended formulations. See the magnetic following load example in chapter 2.

The geometrically exact kinematics and our choice of inner energy allows, however, to consider $\mu_c \to 0$. For $L_c > 0$ it is even possible to choose $\mu_c = 0$, see NEFF [3]. For this case we worked out, that a special term of the curvature $\mathfrak{C}$ can be identified with Nye's curvature, see MÜNCH [4]. Therefore, the additional kinematic $\hat{\mathbf{R}}$ obtains a physical background and can be used to predict zones of initial plasticity.

2. Cone shell with magnetic following load

Volumetric applied twisting moments $\tilde{\mathbf{d}}$ are known from electro- and magnetostatics. Eringen & Maugin [5] define such twisting moments through $\tilde{\mathbf{d}} = \vec{\mathbf{P}} \times \vec{\mathbf{E}} + \vec{\mathbf{M}} \times \vec{\mathbf{H}}$. In general, a material with electric polarization $\vec{\mathbf{P}}$ receives twisting moments within an electric field $\vec{\mathbf{E}}$. The torque of a compass needle is an example for the effect of materials with permanent magnetization $\vec{\mathbf{M}}$ in an outer magnetic field causing $\vec{\mathbf{H}}$. The twisting moment vanishes completely, if the magnetization $\vec{\mathbf{M}}$ of the compass needle is parallel to the outer magnetic field. The twisting moment becomes a maximum, if magnetization and outer magnetic field are perpendicular.

By using the Cosserat rotation field $\bar{\mathbf{R}}$, orientation changes of the polarized or magnetized material can be coupled to the twisting moment in by

$$\mathbf{d} = (\bar{\mathbf{R}}\ \vec{\mathbf{P}}) \times \vec{\mathbf{E}} + (\bar{\mathbf{R}}\ \vec{\mathbf{M}}) \times \vec{\mathbf{H}} \quad . \tag{6}$$

We show this relevance in the following example of a magnetic valve. The valve - a cone shell made of flexible magnetic material[1] - presses its seal onto an o-ring. Shell and seal are remanent magnetized with $\|\vec{\mathbf{M}}\| = B_r = 365.4\,mT$ towards negative z-direction, see Fig. 1. The material is characterized by Young's modulus $E = 300N/mm^2$ and Poisson's ratio $\nu = 0.45$ of isotropic linear elasticity. To simulate a classical elasticity Biot model, the Cosserat parameters are chosen to $\mu_c = \mu$ and $L_c = 0$. With respect to symmetry only a quarter of the system is modeled by 4×6 finite elements in plane and with one element through the thickness. Quadratic shape functions are used, pay attention that the visualization lay a mesh through all nodes.

In xz-plane the displacements in y-direction and the rotations around x- and z-axis are set to zero. Also, in yz-plane the displacements in x-direction and the rotations around y- and z-axis are set to zero. An outer magnetic field causing $\lambda\ \vec{\mathbf{H}}$, which produce in air the magnetic flux density $\lambda\ \vec{\mathbf{B}} \cong 4\,\pi\,10^{-7}\,\lambda\ \vec{\mathbf{H}}$ acts homogeneously to cone and seal. For $\lambda = 1$ the flux density reaches the absolute value of one Tesla. On can produce such a field by a copper wire coil outside the valve. Thus, neither mechanical components nor electrical components are necessary within the valve. Dimensions of the valve can be seen as sectional drawing S1 in Fig. 2. The thickness of the shell amount $t = 0.1\,mm$, the other sizes are $r_1 = 5\,mm$, $r_2 = 10\,mm$, $r_3 = 10.2\,mm$, $r_4 = 11\,mm$, $h_1 = 0.4\,mm$, $h_2 = 0.8\,mm$, $h_3 = 2.4\,mm$.

[1] Elastomer bounded NdFeB-particles, manufactured by Max Baermann GmbH, Germany.

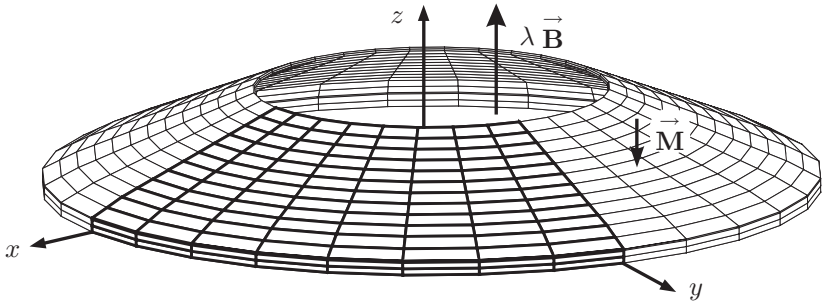

Figure 1: Magnetic cone shell with magnetisation $\vec{\mathbf{M}}$ and action $\lambda\ \vec{\mathbf{B}}$.

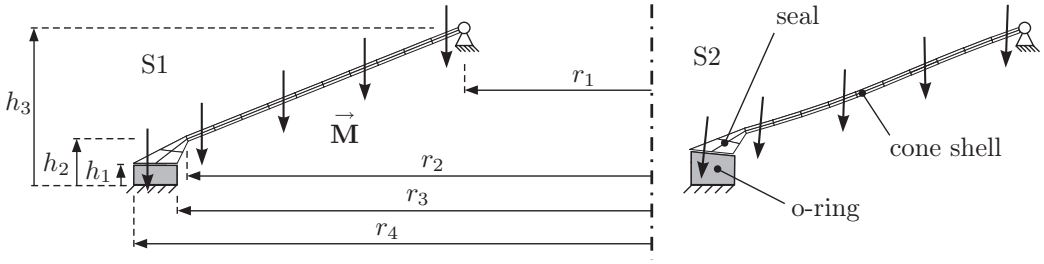

Figure 2: Sectional drawings of the valve in initial state (S1) and for $\lambda = 0$ (S2).

The sectional drawing S1 shows the o-ring (grey) in initial contracted condition. A fictitious force $F_f = 2.1\,N$ compresses the o-ring into this initial position. So, the contact force F_k between seal and o-ring is zero and the cone is undeformed. By removing F_f a natural state of equilibrium appears, as can be seen in the sectional drawing S2 of Fig. 2. In this state, the contact force between seal and o-ring reaches $F_k \cong 1\,N$. Caused by the valve's deformation the direction of the permanent magnetic field $\vec{\mathbf{M}}$ changes. As soon as the seal lift-off from the o-ring, the o-ring is stress free and we measure the height $2.3\,h_1$. That means, the o-ring is compressed in the initial state by the strain $\varepsilon = (h_1 - 2.3\,h_1)/(2.3\,h_1) = -0.57$. For the sake of simplicity, we do not take frictional forces between seal and o-ring into account.

We use the vertical displacement u at the bottom of the seal for the load-displacement diagram in Fig. 3. It is the result of a computation with an arc-length method. Prominent points in the diagram are marked with S1 to S8. In Fig. 2 resp. Fig. 4 every prominent point is shown with its sectional drawing.

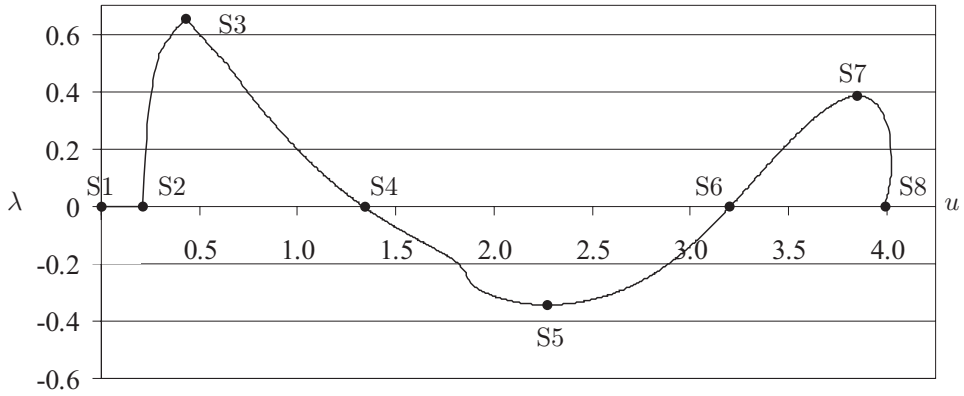

Figure 3: Load-displacement diagram for vertical displacement u from a computation with arc-length method. Prominent points are marked with sectional drawing numbers S1 to S8.

The load-displacement diagram in Fig. 3 shows that standard magnetic flux densities $\lambda \vec{\mathbf{B}}$ are sufficient to open and close the valve. The cone snap-through and remains in open or closed position without outer magnetic fields. With the load factor $\lambda = 0.66$ resp. $\lambda = -0.34$ the valve can be opened or closed. The distance between seal and o-ring is at least $3\,mm$.

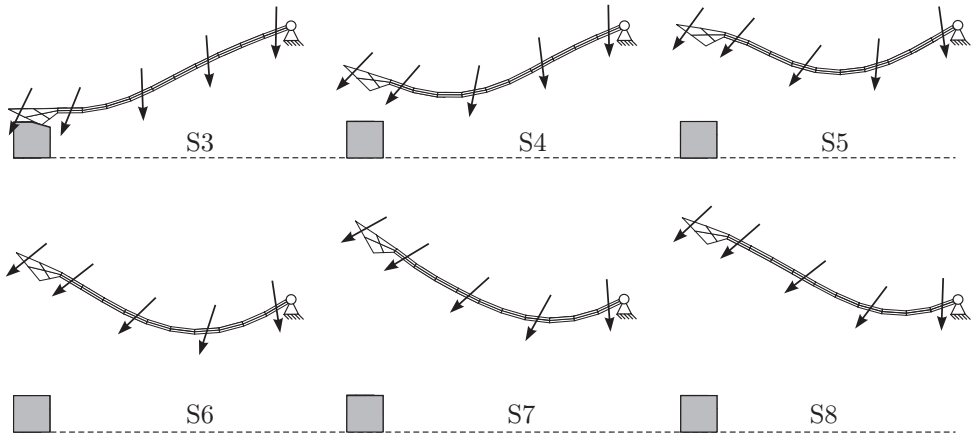

Figure 4: Sectional drawings S3 to S8 corresponding to Fig. 3.

3. Conclusion

We have presented a geometrically exact and materially non-linear Cosserat model. The Cosserat couple modulus μ_c is not a material parameter but rather a modeling parameter. This modulus allows to change completely the simulated physics in the Cosserat model. The parameter combination $\mu_c = \mu$ and $L_c = 0$ realizes a classical Biot model with drilling degrees of freedom whose application is shown in a magnetic following load example. For the parameter combination $\mu_c = 0$ and $L_c > 0$ the Cosserat model is endowed with a true additional kinematic which can be identified with Nye's curvature in defective crystals, see MÜNCH [4].

References

[1] Neff P., Münch I. Curl bounds Grad on SO(3). *ESAIM: Control, Optimisation and Calculus of Variations* 2007; DOI: 10.1051/cocv:2007050

[2] Neff P., Fischle A., Münch I. Symmetric Cauchy-stresses does not imply symmetric Biot-strains in weak formulations of isotropic hyperelasticity with rotational degrees of freedom. *Acta Mechanica* 2007; Published online, 30 October

[3] Neff P. The Cosserat couple modulus for continuous solids is zero viz the linearized Cauchy-stress tensor is symmetric. *ZAMM* 2006; **86**: 892-912

[4] Münch I. Ein geometrisch und materiell nichtlineares Cosserat-Modell - Theorie, Numerik und Anwendungsmöglichkeiten. *Institut für Baustatik* 2007; Dissertation, Berichte (13)

Proceedings of the 6th International Conference on
Computation of Shell and Spatial Structures
IASS-IACM 2008: “Spanning Nano to Mega”
28-31 May 2008, Cornell University, Ithaca, NY, USA
John F. ABEL and J. Robert COOKE (eds.)

Utilization of the assumed natural strain method in a surface-related solid-shell element

Bernd W. ZASTRAU*, Rainer SCHLEBUSCH

*Faculty of Civil Engineering
Institute of Mechanics and Shell Structures
Technische Universität Dresden
D-01062 Dresden, Germany
E-mail: Bernd.Zastrau@tu-dresden.de

Abstract

The numerical simulation of thin textile reinforced concrete (TRC) strengthening layers is the object of this research. Its mechanical description is implemented by a shell formulation demanding an efficient numerical solution strategy. The shell model is formulated with respect to one of the outer surfaces, i.e. the shell formulation is surface-related. The discretization and interpolation of the associated variational formulation are sources of several locking phenomena. Extensions and/or adjustments of well-known techniques to prevent or at least to reduce locking like the assumed natural strain (ANS) method and the enhanced assumed strain (EAS) method have to be made. In particular, the ANS method is investigated and adapted to reduce transversal shear locking and curvature thickness locking in this contribution.

1. Introduction

In the context of the Collaborative Research Center 528 "Textile Reinforcement for Structural Strengthening and Repair" at the Technische Universität Dresden a surface-related solid-shell element is developed for the mechanical simulation of textile reinforced fine-grained concrete strengthening layers. With respect to that framework of application, it is taken advantage of the in principle free choice of the reference surface position by attaching the reference surface to one of the outer surfaces (Schlebusch *et al.* [7]), (Schlebusch [6]) and (Schlebusch & Zastrau [8]). The degeneration concept alone does not permit the usage of three-dimensional constitutive relations, if for the semi-discretization of the displacement field a linear series expansion is used. But in combination with the EAS method, its application becomes possible (Büchter & Ramm [4]). This combination comprises a shell formulation with a minimal number of kinematical degrees of freedom necessary to operate with complete three-dimensional constitutive relations (Bischoff & Ramm [3]) and is adapted for a surface-related formulation.

2. Shell Formulation

The key assumption of the utilized shell formulation concerns the kinematics. The displacement field $\boldsymbol{U}$ of the shell body is assumed to be linear through the thickness of the shell

$$\boldsymbol{U} = \boldsymbol{V} + \Theta^3 \boldsymbol{W} \,, \tag{1}$$

wherein $\boldsymbol{V}$ represents the displacement field of the reference surface and $\boldsymbol{W}$ describes the movement of the so-called shell director $\boldsymbol{D}$. Corresponding to the particular position of the reference surface, it follows for the thickness coordinate Θ^3 to be in the interval [0,1].

3. Element Formulation and Locking

Probably the major drawback of the chosen linear shell kinematics is that it suffers from Poisson thickness locking in bending dominated problems, since the kinematics produces only constant transverse strains E_{33}. The

necessary introduction of linear strains is achieved by aid of the EAS method. This formulation was originally proposed by Büchter & Ramm [4] and has to be adapted to the particular position of the reference surface. This adaptation was realized in Schlebusch & Zastrau [8]. Additionally to Poisson thickness locking, the following locking phenomena may occur: transverse shear (out-of-plane), curvature thickness, membrane, shear (in-plane) and volume locking.

An effective concept against transverse shear locking, see Dvorkin & Bathe [5] and Bathe & Dvorkin [1], and against curvature thickness locking, (Betsch & Stein [2]), is given by the ANS method. To prevent or reduce membrane, shear and volume locking, the EAS method is also used again. The details for the necessary extensions and/or adjustments of the EAS method for utilization in a surface-related shell formulation can be found in the Ph.D. thesis (Schlebusch [6]) and in (Schlebusch & Zastrau [8]).

3.1 Displacement-Compatible Strains

Due to the used bi-linear interpolation of $\boldsymbol{V}$ and $\boldsymbol{W}$ the element is able to represent several deformation modes, but the number is always limited to the finite element's number of degrees of freedom, i.e. to 24. Hence, the purpose of this work is to develop a surface-related solid-shell element capable of representing well defined deformation modes like pure bending and bending of a curved element in both linear and non-linear simulations. To investigate this problem a fictitious[1] about the X^1-axis curved finite element in the reference configuration is examined, see Figure 1. The considered element has a flat rectangular reference surface with the dimensions $2L$ and $2B$ in the X^1 and X^2 direction and a "constant thickness" H.

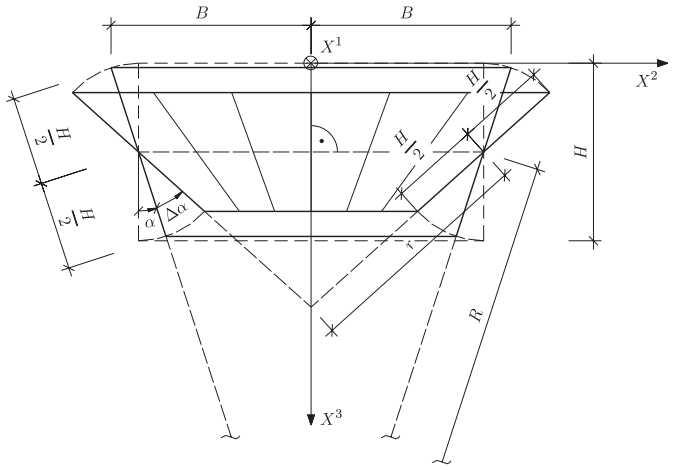

Figure 1: Bending of a fictitious about the X^1-axis initially curved finite element in the reference (radius of curvature R) and deformed configuration (radius of curvature r)

The bending deformation is defined by the angle $\Delta\alpha$. The angle $\Delta\alpha$ needs not to be small. Large deformations and therewith non-linear strains are particularly allowed. The only non-vanishing tensorial components of the displacement compatible strain tensor are E_{22h}, E_{23h} and E_{33h}. For the evaluation of the interpolated components E_{22h}, E_{23h} and E_{33h}, the strain tensor for the exact Kirchhoff-Love kinematics, see figure 2, is supplementarily investigated.

[1] The term "fictitious" is used, since the considered element, i.e. its reference surface, has no curvature in the meaning of differential geometry.

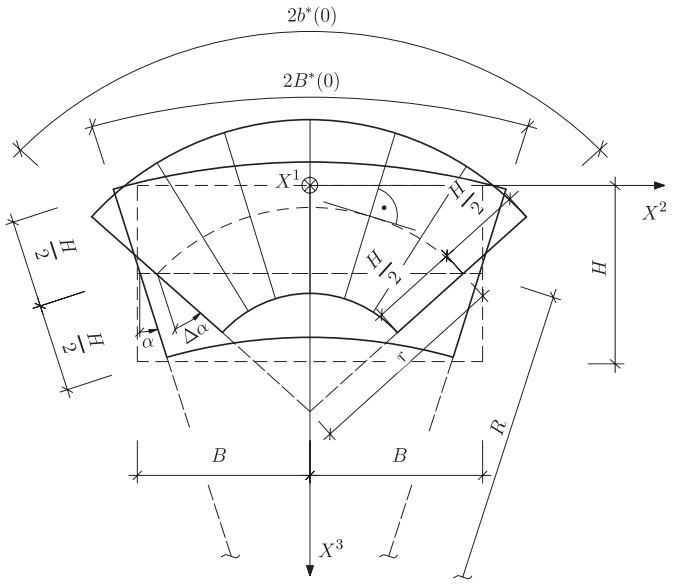

Figure 2: Bending of an about the X^1-axis initially curved shell in the the reference (radius of curvature R) and deformed configuration (radius of curvature r)

As expected only the longitudinal stretches E_{22} are present. Consequently, E_{23h} and E_{33h} have not to be present in a pure bending deformation. The existence of shear strains induced by a pure bending deformation causes so-called transversal shear locking and the existence of parasitical transversal stretches causes so-called curvature thickness locking. However, the condition of vanishing transversal strain E_{23h} is fulfilled for $\Theta^2 = 0$ and every Θ^3. The condition of vanishing transversal E_{33h} is fulfilled for $\Theta^2 = \pm 1$ and every Θ^3.

3.2 Reduction of Artificial Stiffening Effects

In general, there exist two ways to reduce or even to eliminate in some special cases the locking behavior of finite elements. Either these parts being responsible for the parasitical stresses and strains are eliminated from the formulation or those parts being necessary for a balanced interpolation of stresses and strains are supplemented. The elimination of the parasitical stresses leads among others to the selective reduced integration method, to the ANS method or to the discrete shear gap (DSG) method. The supplement can be implemented by the method of incompatible modes or by the EAS method. A balanced selection of the methods is extremely important to receive a most efficient element formulation. Since every enhancement or supplement of the formulation generally increases the numerical effort, it should principally be chosen a reducing method to eliminate locking causing parts.

3.3 The Assumed Natural Strain Method

This method attempts to eliminate parasitical strains by modifying and replacing the displacement compatible strain field responsible for the artificial stiffening behavior.

(a) Transverse Shear Locking

The ANS method is based upon the observation that the parasitical shear strains vanish in some points or cross section in the finite element. Those points yielding shear strains without any parasitical strains for a pure bending deformation are therefore used as collocation points for an interpolation of the shear strains over the element. Hence, this method is based upon the observation that was made at the end of Chapter 3.1.

Considering thin shells, i.e. $B \gg H$, the influence of the parasitical strains is even amplified, since the shear stiffness increases proportional to the thickness H and the bending stiffness proportional to H^3. Consequently,

the shear stiffness dominates more and more the bending stiffness resulting in an artificial overestimation of the element's stiffness in bending dominated load cases. The overestimation of the stiffness reduces with an increase of the fineness of the discretization, since for $B \to 0$ and therewith $\Delta\alpha \to 0$ the parasitical strains E_{23h} respectively vanish for $\Delta\alpha \to 0$.

(b) Curvature Thickness Locking

Curvature thickness locking only occurs in shell formulations allowing through the thickness deformations and using simultaneously a shell kinematics without rotation variables (Betsch & Stein [2]). Curvature thickness locking and thickness locking as well are consequences of the six parameter shell kinematics. The poor interpolation of the transversal stretches E_{33h} are responsible for curvature thickness locking.

Curvature thickness locking only occurs in geometrically linear simulations, if the element has a fictitious curvature in the reference configuration, characterized by the angle α in Figure 1. Nevertheless, curvature thickness locking occurs in geometrically non-linear simulations, even if the element has no fictitious curvature in the reference configuration. Again, the overestimation of the stiffness decreases with an increase of the fineness of the discretization for both linear and non-linear simulations, since for $B \to 0$ and therewith $\Delta\alpha \to 0$ the parasitical stretch E_{33h} vanishes.

4. Conclusions

Using adapted methods, like the EAS and ANS method, a reliable surface-related solid-shell element with tremendously reduced locking properties is obtained. This concept comprises the utilization of unmodified three-dimensional constitutive relations by a minimal number of kinematical parameters. Due to the particular position of the reference surface, well-established techniques against locking phenomena are extended and/or adjusted.

Acknowledgements

The authors gratefully acknowledge financial support of this research from Deutsche Forschungsgemeinschaft DFG within the Sonderforschungsbereich SFB 528 "Textile Reinforcement for Structural Strengthening and Repair" at the Technische Universität Dresden.

References

[1] Bathe KJ and Dvorkin EN. A Four-Node Plate Bending Element Based on Mindlin/Reissner Theory and a Mixed Interpolation. *International Journal for Numerical Methods in Engineering* 1985; **21**:367-383.

[2] Betsch P and Stein E. An Assumed Strain Approach Avoiding Artificial Thickness Straining for Non-Linear 4-Node Shell Element. *Communications in Numerical Methods in Engineering* 1995; **11**:899-909.

[3] Bischoff M and Ramm E. Shear Deformable Shell Elements for Large Strains and Rotations. *International Journal for Numerical Methods in Engineering* 1997; **40**:1-23.

[4] Büchter N and Ramm E. 3D-Extension of Nonlinear Shell Equations Based on the Enhanced Assumed Strain Concept. In *Computational Methods in Applied Sciences: Special Technological Sessions of the First European Computational Fluid Dynamics Conference and the First European Conference on Numerical Methods in Engineering*, Hirsch C, Periaux J, Oñate E. (eds). Elsevier: Oxford, 1992; 39-59.

[5] Dvorkin EN and Bathe KJ. A Continuum Mechanics Based Four-Node Shell Element for General Nonlinear Analysis. *Engineering Computations* 1984; **1**:77-88.

[6] Schlebusch R. Theorie und Numerik einer oberflächenorientierten Schalenformulierung. Ph.D. thesis, Technische Universität Dresden, Institute of Mechanics and Shell Structures, Dresden, 2005.

[7] Schlebusch R, Matheas J, Zastrau. B. On Surface-Related Shell Theories for the Numerical Simu-lation of Contact Problems. *Journal of Theoretical and Applied Mechanics* 2003; **41**:623-642.

[8] Schlebusch R and Zastrau B. Theory and Numerics of a Surface-Related Shell Formulation. In *Third European Conference on Computational Mechanics*, Soares CAM, Martins JAC, Rodrigues HC, Ambrósio JA (eds). Springer: Dordrecht, 2006; 16 pages.

Proceedings of the 6th International Conference on
Computation of Shell and Spatial Structures
IASS-IACM 2008: "Spanning Nano to Mega"
28-31 May 2008, Cornell University, Ithaca, NY, USA
John F. ABEL and J. Robert COOKE (eds.)

Dimensional adaptivity in finite element simulation of sheet metal forming

Dmitry LEDENTSOV*, Alexander DÜSTER, Ernst RANK, Ingo HEINLE, Wolfram VOLK, Marcus WAGNER

*Lehrstuhl für Computation in Engineering,
Technische Universität München
Arcisstr. 21
80290 München, Germany
ledentsov@bv.tum.de

Abstract

This paper provides an outlook of a scheme for dimensional adaptivity based on a model error indicator, applied to sheet metal forming simulations.

1. Introduction

Sheet metal forming is a widely applied manufacturing technique in the automotive industry. Large production volumes and high tooling costs drive the need for robust and inexpensive forming simulations. Such simulations are usually performed using dimensionally reduced finite element formulations, such as shell elements. These provide forming simulations at a comparatively low computational cost and support easy modeling. However, modern demand for complex geometric shapes often poses significant challenges for modeling and simulation. Due to model assumptions of shells, many local material behavior effects cannot be represented, which can lead to wrong interpretation of simulation results and cause high tool rework costs. However, due to the complexity and size of the models used, deep drawing simulation using three-dimensional solid elements has proved to be too expensive in industrial engineering practice. Model-adaptive techniques can provide a cost-effective approach to capture local three-dimensional effects while employing reduced finite element formulations for non-critical parts of the computational domain.

2. Model error indicator

2.1 Model adaptivity in context of sheet metal forming

Various authors have recognized the need for estimating the simulation error caused by the introduction of model assumptions into the discretized model (i.e. Schwab [6], Stein and Ohnimus [7]). Proposed model error estimators are formulated for linear elastic problems and are mostly based on model hierarchy. Model adaptivity is typically performed in the direction of model reduction (Stein and Ohnimus [7]) – by starting with a highest appropriate model, and performing model reductions for further analyses, driven by an a-posteriori model error estimation. In context of sheet metal forming simulation, being a nonlinear elastic-plastic analysis with complex geometries and changing contact surfaces, a model enhancement technique is more suitable.

2.2 Domain decomposition

The approach for model error estimation is based on the hierarchic domain decomposition (*hp-d* method) as proposed by Rank [5]. The *hp-d* method has been extended to locally enhance dimensionally reduced models (Düster [2], Düster *et al.* [3]) and to couple linear and nonlinear models in soil mechanics (Düster, *et al.* [3]). Here we extend the idea of the *hp-d* method to large deformations in order to localize and quantify the model error in a fully nonlinear sheet metal forming analysis. The implementation of the method presented below relies upon the commercial finite element code ABAQUS [1] to ensure applicability to large industrial models.

2.3 Forming analysis

The nonlinear forming analysis including contact and finite elastoplastic deformations is performed by applying a dimensionally reduced finite shell formulation based on Reissner-Mindlin kinematics. The deformation of the shell model is the starting point for a fully three-dimensional simulation based on hexahedral solid elements.

2.4 Model conversion

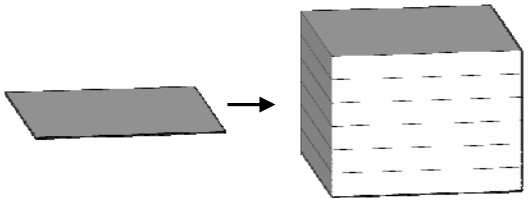

Figure 1: Conversion of a quadrilateral shell element into a stack of hexahedral elements

The solid discretization of the work piece is generated from the shell model via extrusion of shell elements (mid-surfaces) into stacks of solid elements, taking into account the shell thickness.

2.5 Displacement driven simulation

After the model conversion, the displacements of the shell model are applied to the mid-surface of the fully three-dimensional solid discretization and a corresponding three-dimensional nonlinear simulation is carried out. Due to the nonlinearity of the forming analysis, the displacements are applied incrementally as sketched in Figure 2. Based on the three-dimensional discretization, a displacement driven boundary value problem is solved without the incorporation of the contact analysis. The solid elements model yields a fully three-dimensional stress state and the corresponding results are used to indicate those regions where a significant model error appears. Since the three-dimensional discretization is just applied for error indication, the corresponding simulation does not need to be carried out for every displacement increment, reducing the computational effort accordingly.

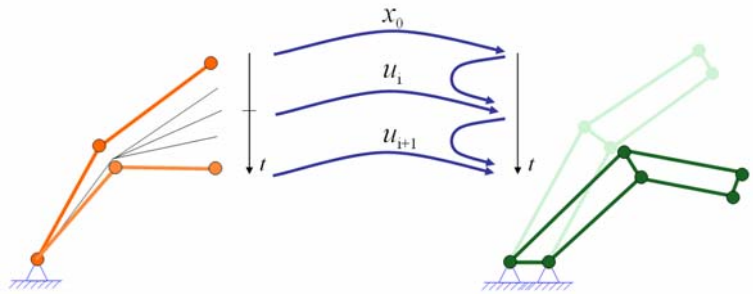

Figure 2: Incremental projection of the deformation path from a shell model onto a solid model

2.6 Model error indicator

Contact forces act in the thickness direction of the metal sheet, influencing the thinning of the metal sheet locally. This, nevertheless, has an impact on global geometric values, such as spring-back angles. In the shell model however, thinning is only computed from the in-plane strains, thereby neglecting the influence of local three-dimensional effects, such as accumulation of material near a sharp tool tip, i.e. a tool with a radius comparable or smaller than the thickness of the sheet metal.

In order to detect those regions where a significant model error appears, we propose to consider the normalized thickness difference a_t (eqn. 1) between the shell model t_{shell} and the solid model t_{hex}. To this end, the model error indicator a_t is computed based on the original forming analysis and the displacement-driven analysis as outlined in the previous section. The scaling thickness t_0 has been set to the initial thickness of the metal sheet.

$$a_t = \frac{\left| t_{shell} - t_{hex} \right|}{t_0} \tag{1}$$

In order to demonstrate the performance of the error indicator, consider the deep drawing of a metal sheet as depicted on the left-hand side of Figure 3. The error indicator has been computed as described above and the corresponding result is plotted on the right-hand side of Figure 3. From this it can be seen that regions with small radii are indicated, where the shell elements are expected to deviate from a fully three-dimensional stress state. The error indicator has then been used to drive the selective re-meshing of the work piece using an automated procedure as described in the subsequent Section 2.7.

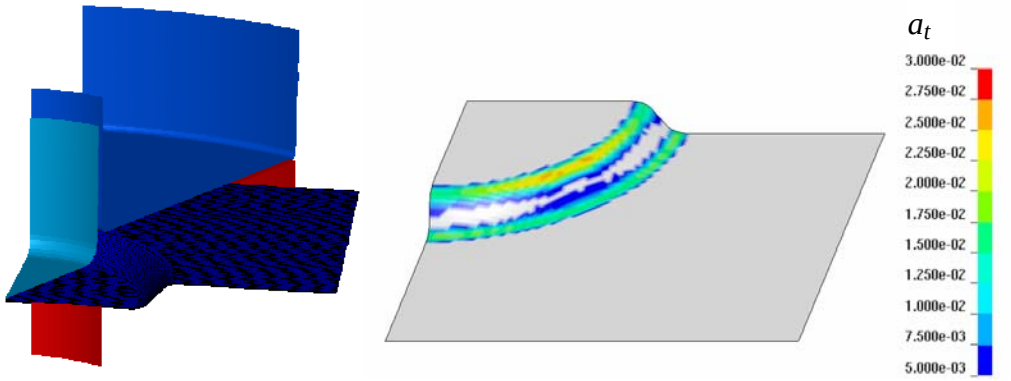

Figure 3: Deep-drawing of a metal sheet (left), Model error indicator (right)

2.7 Model-adaptive re-meshing

Based on the model error indicator outlined above, the initial discretization of the metal sheet is converted from shell to solid elements in critical, i.e. indicated regions. In order to avoid disturbances at mesh transitions between solid and shell elements, the critical region is further increased. To this end, an automatic selective extrusion of shell elements is performed. Additionally, appropriate coupling conditions between the shell and solid element regions are taken into account during the selective mesh extrusion (ABAQUS [1]).

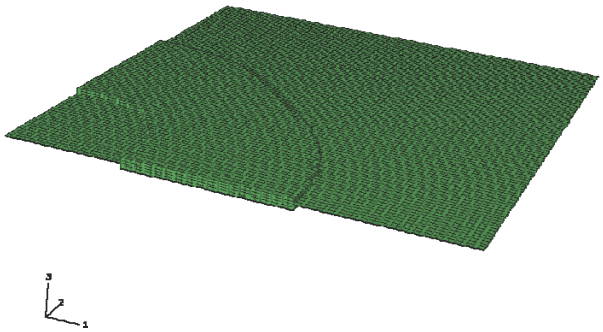

Figure 4: Automatic re-meshing of a part driven by the model error indicator

Figure 4 depicts a selectively extruded mesh in the initial geometry for the model shown in Figure 3. The mixed mesh can be then used in a forming analysis with the original contact conditions.

3. Results

In this section, the results of a simple model-adaptive computation are presented in order to illustrate the potential influence of the model error on the accuracy. On the left-hand side of Figure 5, one can see the schematic simulation set up. The metal strip (a) is held between two tools (b,c), and is bent by the third tool part (d). In a first step, the work piece has been discretized and computed with shell elements. The model error has

then been computed as outlined in sections 2.4-2.6. A model-adaptive solution has been performed with the same contact boundary conditions as in the shell model. Finally, a fully-hexahedral discretization has been computed serving as a reference. The final position of the tip of the metal strip is of interest. On the right-hand side of Figure 5 the final positions of the metal strip are shown for all three discretizations.

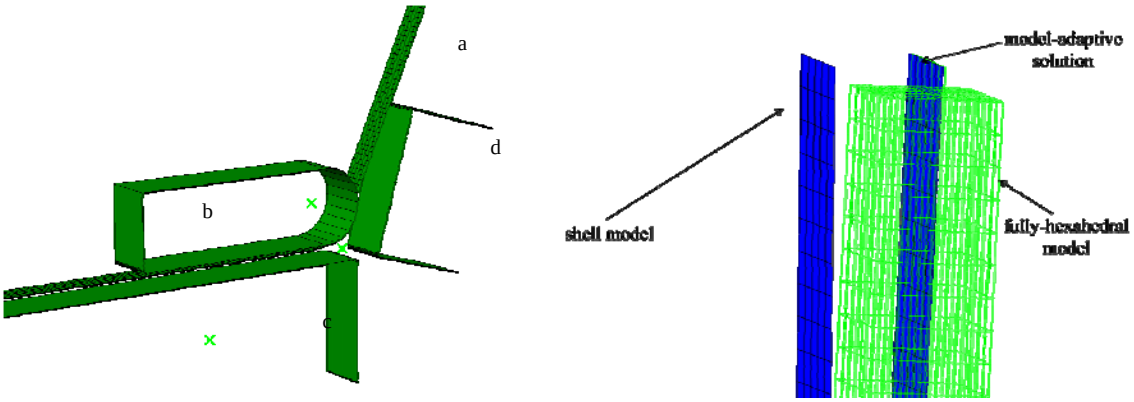

Figure 5: Model-adaptive computation of a simple bending model

The model-adaptive solution almost coincides with the reference solution, while the final position of shell model tip lies considerably off the reference solution.

4. Conclusions

An outline for a model-adaptive analysis technique, based on a model indicator has been presented. The error indicator and the automated selective mesh extrusion and coupling schemes have shown to yield accurate results. Future work will concentrate on further investigation of the model indicator.

References

[1] ABAQUS Version 6.6 Analysis User's Manual

[2] A. Düster, High order finite elements for three-dimensional thin-walled nonlinear continua, Ph.D, thesis, *Lehrstuhl für Bauinformatik, Fakultät für Bauingenieur- und Vermessungswesen, Technische Universität München*, 2001

[3] A. Düster, A. Niggl, E. Rank, Applying the hp-d version of the FEM to locally enhance dimensionally reduced models, *Computer Methods in Applied Mechanics and Engineering*, 196:3524-3533, 2007

[4] A. Düster, E. Rank, G. Steinl, W. Wunderlich, A combination of an h- and p-version of the finite element method for elastic-plastic problems, *Proceedings of ECCM '99, European Conference on Computational Mechanics, München, Germany*, 1999

[5] E. Rank, Adaptive remeshing and h-p domain decomposition, *Computer Methods in Applied Mechanics and Engineering*, 101 (1992) 299-313.

[6] C. Schwab, A-posteriori modelling error estimation for hierarchic plate models, *Numer. Math. 74: 221-259 (1996)*, Springer-Verlag, 1996

[7] E. Stein, S. Ohnimus, Coupled model- and solution-adaptivity in the finite element method, *Computer Methods in Applied Mechanics and Engineering*, 150 (1997) 327-350